Liquid crystal elastomer–nanoparticle systems for actuation

Martin Chambers,[*ab] Heino Finkelmann,[c] Maja Remškar,[a] Antoni Sánchez-Ferrer,[cd] Boštjan Zalar[ae] and Slobodan Žumer[ae]

Liquid crystal elastomers (LCE) are currently of great interest due to conjoining of mesogenic ordering and rubber elasticity, exhibited in their large spontaneous thermally stimulated changes in shape. It has been shown that nanoparticles (nanotubes, photo-isomerisable dyes, magnetic nanoparticles…) can be incorporated into these LCE networks to create a more sensitive network to external stimuli (i.e. strain or stress, optical, electrical, electro-thermal, magnetic…). Here, we briefly summarise the current state of LCE–nanoparticle systems and explain in detail one system utilising carbon nanoparticles integrated at surfaces that may be used for electro-thermal heating of LCE systems.

[a]*J. Stefan Institute, Jamova 39, SI-1000 Ljubljana, Slovenia. E-mail: MChambers@ijs.si*
[b]*Physics Department, Kent State University, Kent, Ohio, 44240, USA*
[c]*Institute for Macromolecular Chemistry, University of Freiburg, Stefan-Meier-Str. 31, 79104 Freiburg, Germany*
[d]*Department of Physics, University of Fribourg, Chemin du Musée 3, 1700 Fribourg, Switzerland*
[e]*Department of Physics, University of Ljubljana, Jadranska 19, SI-1000 Ljubljana, Slovenia*

1. Introduction

Liquid crystal elastomers (LCEs) exhibit changes in their macroscopic shape due to the interaction of the mesogenic and elastic polymer components,[1] exhibiting liquid crystallinity, elasticity and their interplay. Liquid crystal elastomers systems were created over 20 years ago and much of the thermal behaviour is understood well with thermally stimulated length changes of up to 400%.[2] The major exploitable physical characteristic of LCEs, their unusually large thermomechanical response, is driving numerous application-oriented activities.[3] One current problem, however, is how to create or reprocess LCE systems into a form that can be easily utilised whilst preserving the thermo-mechanical properties. In general, this electro-mechanically responsive, with a limitation of slow response times. More recently, by application of a high electric field across a smectic LCE[10] bending motions have been induced by the electroclinic effect (direct coupling of molecular tilt in the smectic layer to applied field) with reasonable rates of response at relatively low voltages.

In thermo-mechanical actuation, the most simple solutions include the use of flexible conducting wires,[11] optical absorption of light using a single sprayed adsorbing layer,[12] or deformable conducting polymer plates that are resistively heated. Typically these types of approaches also have significant heat transfer problems, cause mechanical restriction as well as quick degradation due to large temperature gradients and mechanically incompatible parts. Carbon nanotube loaded LCE can also be actuated *via* opto-thermal compression of nanotubes.[13] More recently, it has be shown that indirect heating mechanisms can be used, such as using LCE incorporating magnetic particles,[14] where the magnetic field provides for vibration of the particles and creates local heating of particles in the LCE network.

The basic theoretical descriptions of LCE are well developed and stem from liquid crystal and polymeric statistical approaches with the use of the elastic descriptions similar to that of rubbers.[1] Much of the thermal behaviour is understood well, as are the elastic and strain contributions to the dynamical and static requires the functionalisation or addition of nanosized particles to instil properties in the LCE that can be altered rapidly by external stimuli. Various methods can in principle be used to induce changes in geometrical shape such as opto-mechanical, electro-mechanical or thermo-mechanical actuation.

Opto-mechanical actuation directed towards direct optical to mechanical conversion can be performed through the use of photoisomerisable dyes,[4] incorporated into the network. Mostly simple azobenzene dyes are chemically crosslinked,[4] but they may also be dissolved into the network,[5] liquid crystalline in nature, or even used as the crosslinker. In general, the response time is on the order of minutes to hours, where the relaxation speed is similar and both are dependent on temperature. In polydomain LCEs, polarised light may also be used to control the direction of the shape changing response[6] by selective adsorption in suitably aligned domains with respect to the optical polarisation direction. How and where the heat is generated and whether it is significant in this process is still an open question.

Electro-mechanical actuation effects have been observed in ferroelectric liquid crystal elastomers[7] and low molecular-mass nematogen-swollen LCEs.[8] LC-like response times were observed, however with rather small elongational response. Carbon nanotube/LCE composite materials[9] can also be made orientational and positional ordering of LCE systems.[1] Simulation of LCE, where the complete director may be rotated, predicts LCE shape changes like up to 500% elongation. Simulations of existing known effects such as photo-mechanical response of LCE systems can replicate the observed behaviour and possible new phenomena.[15] Theoretical predictions on new phenomena have been provided such as biaxial[16] and ferroelectric[17] LCE behaviour. Additionally, finite element modelling allows for a coarse-grain simulation of themo-mechanically induced response of prototype systems, *e.g.* mimicking of actions of moving worms or snakes.[18]

Our approach was to investigate a method to create a conducting LCE system which can be resistively heated. Effectively conducting systems can be created using surface conducting layers. Homogeneous metallic layers lack the robustness to perform large deformations without patterning[19] and the use of these rigid layers restricts movement. Materials where a secondary particulate conducting composite component (*e.g.* isotropic PDMS and conducting particles) is deposited at the surface typically suffer from quick degradation. A thick sprayed layer of conducting carbon particles also can result in a loss of the LCE[12] mechanical response. Other possible methods using the redox of metal salts[20] are not attractive possibilities. Preparation of composite materials using conducting nano-particles

such as carbon and gold is also not possible at concentrations required for high conductivity as the system elasticity is drastically altered. Composite LCE structures using nanotubes[5,13] can show low resistivity at low concentration but the macroscopic elasticity is also influenced significantly. An effectively conducting system can be created[21–23] without loss of mechanical response through a swelling technique. The procedure consists of placing a swollen LCE network in a suitable solvent containing dispersed carbon particles. The subsequently deswollen LCE network exhibits an effective conductance. Here, the mechanism and process are illustrated as well as control over it. Additionally, conductive layers on elastic substrates are interesting for many additional applications such as interconnects,[24] sensors[25] or flexible heating elements.[26]

2. Preparation of carbon-black-reprocessed LCE networks

2.1 Materials

The elastomer networks used here are side-chain (SC) LCEs, composed of a poly[oxy(methylsilylene)]-based backbone, a mesogen, and a crosslinker (10%), as shown in Fig. 1a. They exhibit an isotropic–nematic phase transition $T_{NI} \approx 80$ °C, whereas the glass transition occurs at −4 °C. Nematic monodomain samples are prepared by the "Finkelmann procedure".[27] Individual pieces measuring roughly $10 \times 1 \times 0.3$ mm^3 were cut from the LCE specimen. To create a conducting LCE, a conducting component, carbon black, was used. Carbon black[28] (Printex XE2, Degussa, denoted CB) can be described as approximately spherical particles with a 30 nm average diameter.

2.2 LCE response to swelling

A property of LCE systems in anisotropic[29,30] and isotropic[30,31] solvents is their ability to swell. Similar to common elastomers, the behaviour in monodomain LCEs, when placed in a suitable solvent, may be explained by the Flory–Huggins free energy minimisation.[29,30] In particular, the sum of elastic and mixing energies of a polymeric gel, swollen in a solvent, is minimised with respect to the relative elastomer volume V/V_0. Its equilibrium value is determined by X (Flory–Huggins interaction parameter) and excluded volume, v. The former depends on solvent interaction with the network, whereas the latter is controlled by structural parameters like crosslinking density and domain properties of the LCE network. When a LCE is placed in

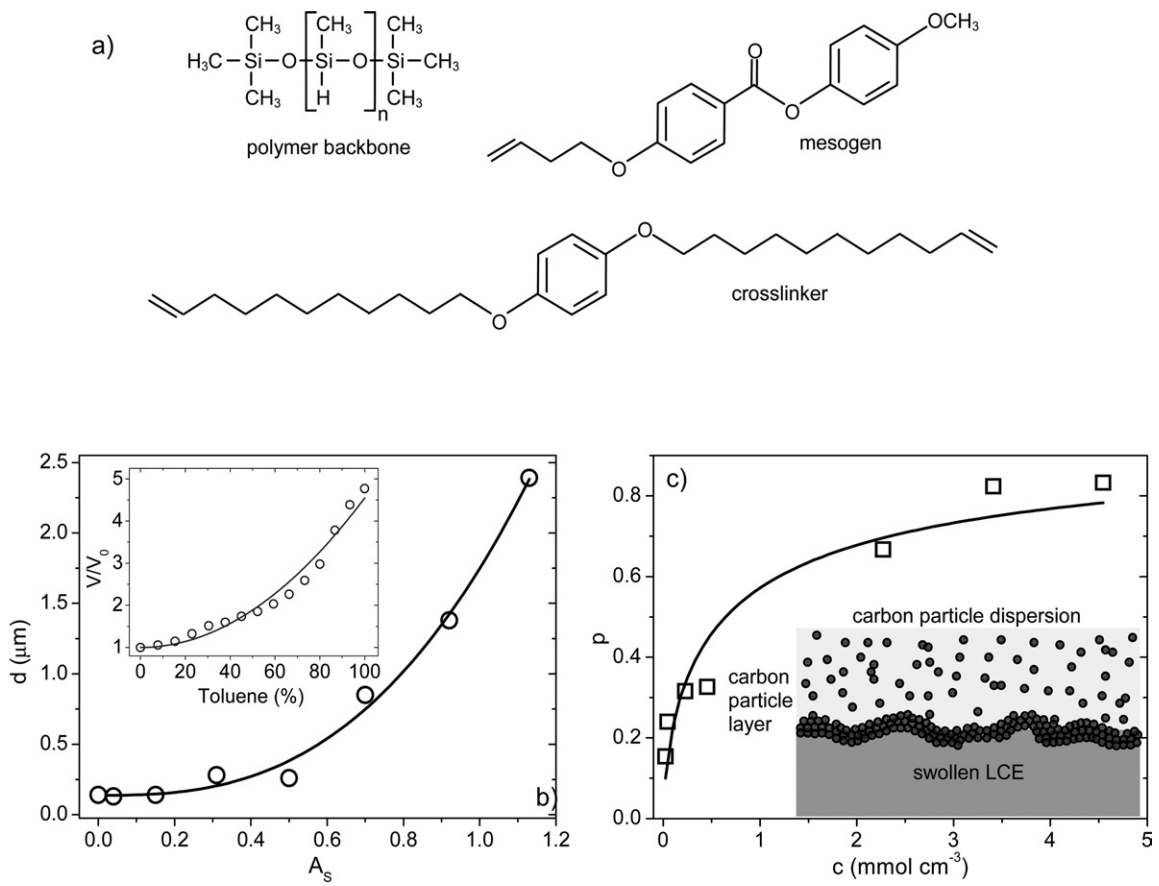

Fig. 1 a) Typical building units of a conventional side-chain liquid crystal elastomer. b) Layer thickness, d, vs. surface expansion ratio, A_S, of a carbon black reprocessed sample (circles) where the surface expansion ratio of the side-chain LCE sample was controlled through swelling (cyclohexane–toluene mixtures). The inset shows the LCE relative volume, V/V_0, response (circles) when the cyclohexane solvent is replaced with toluene. The best fit curve (line) is a power function with exponent 2 as predicted by the Flory–Huggins interaction parameter term. c) Particle fraction, p, vs. concentration, c, for carbon black (squares). The best fit lines of the Langmuir equation are also shown. A graphical representation of the swollen LCE in a high concentration carbon particle dispersion, where a surface adsorbed layer is formed at all exposed surfaces, is shown in the inset.

a cyclohexane solvent, little volume change is observed. If a toluene solvent is used, the LCE becomes expanded in volume, as the solubility term, X, increases in magnitude. The relative volume increase with increasing toluene concentration in a cyclohexane–toluene mixture is shown in Fig. 1b inset. The V/V_0 increases with the square of the solubility change as suggested in the Flory–Huggins parameter without discontinuities, allowing for control over the relative volume and surface area.

3. Reprocessing technique analysis

If the average distance between the LCE crosslinks is taken to be representational of the size to which non-interacting and soluble particles may penetrate a polymer, it is of the order of 10 nm. If the LCE network is expanded by swelling, the increase in volume is typically 400% for the samples used here. Therefore, the CB particles themselves are not able to penetrate the LCE network as they are far too large and insoluble in the solvents used here. One characteristic of CB is that the particles have a high surface area, therefore the inter-particle attractions (agglomeration)[28,32] as well as particle–polymer interactions[33] are significant. CB is typically used for conducting polymeric systems due to the percolative nature of the conducting network formation that results in a low weight percent conductivity. The "substrate" used in our studies, i.e. the polymeric silicone, also has good adsorptive properties.[34]

To describe the adsorption of particles from a solution onto a solid substrate,[35] Langmuir theory is commonly used. The surface coverage fraction ζ ($0 \leq \zeta \leq 1$) can be defined by the particle concentration, c, and the equilibrium rate between adsorption and desorption, k_E. A more general formula, given in reference 36, which applies to various types of isotherms, is Eq. 1:

$$\zeta = (k_E c)^{\alpha}/(1 + (k_E c)^{\alpha}) \quad (1)$$

Here, α is a heterogeneity parameter. The general property of the absorption process described by the above equation is the increase of surface coverage value with increasing concentration c.

3.1 Variation in concentration

An explanation of the decay in resistivity vs. carbon particle concentration is that when the LCE is expanded in volume, the surface is exposed to carbon particles. The carbon particles become adsorbed to the LCE expanded surface. This results in the formation of adsorbed carbon particles over any exposed LCE surface. When the LCE is deswollen, the expanded LCE contracts to its unexpanded conditions, resulting in the formation of a integrated LCE–carbon surface layer. The decay in resistivity may be described by a Langmuir type isotherm for monolayer formation, where the average layer resistivity varies with an assumed fixed layer thickness. The surface coverage value in the swollen state is increasing with particle concentration, therefore the integrated layer can also be described by lattice percolation theory, as there effectively exists a fixed volume of LCE where the particle concentration is increasing. The relative change in resistivity[37] ρ depends on the electrical percolation threshold p_c, critical exponent κ, and conducting particle fraction p, as shown in Eq. 2:

$$\rho/\tilde{\rho} \propto (p + p_c)^{\kappa} \quad (2)$$

The carbon particulate values of $\tilde{\rho}$ are already well known,[28,38] as well as p_c and κ values of LCE–carbon particle composites.[28,37–39] For the measured resistivity values, this allows for the estimation of the conducting particle fraction that corresponds to $p \approx 80\%$ wt. in the integrated layer at the saturated concentration level. Taking that the local volume fraction p is related to the monolayer coverage fraction, the Langmuir adsorption is shown in Fig. 1c.

3.2 Variation in surface expansion ratio

The LCE surface expansion ratio can be controlled through variation in the solvent–LCE solubility by use of cyclohexane and toluene mixtures. The LCE system was processed at a constant concentration of carbon particles relating to the saturated region exhibited in Fig. 1c in a pure toluene solvent. To examine the interior of the LCE and surface layer thickness, reprocessed LCE were flushed after removal from the carbon particle dispersed solvent, using pure solvent to remove any excess particles on the surface. The flushed LCE were then cryogenically frozen in liquid nitrogen and brittle-fractured in air. These pieces were then examined using scanning electron microscopy (SEM). From SEM images (Fig. 2a), it can be seen that there is a layer with an average thickness of around 2 μm and

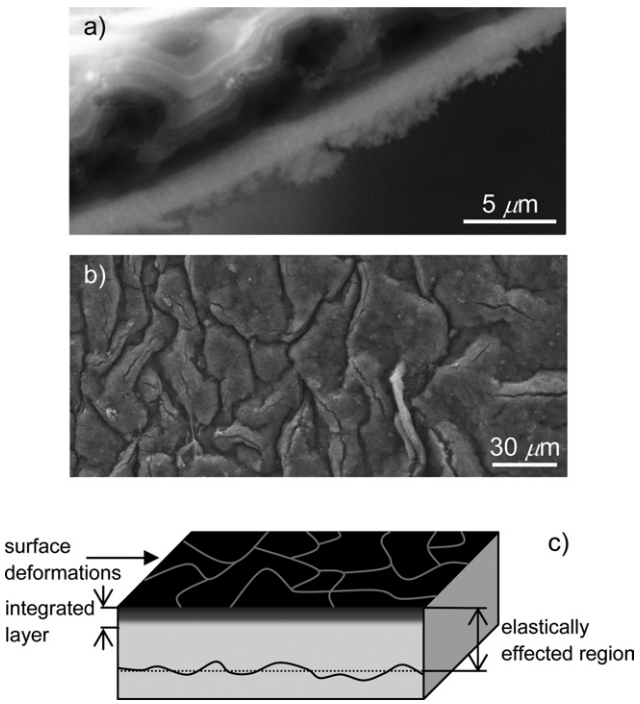

Fig. 2 a) SEM image of a carbon black reprocessed freeze fractured side-chain LCE sample. The surface conducting layer can be observed as the grey band running from bottom left to top right in the image. The conducting layer thickness is around 2 μm. b) SEM image of the LCE surface, showing affects of buckling. c) Graphical image of the observed effects of the integrated layer thickness, irregular surface buckling appearance and an elastically effected region that extends into the LCE bulk.

additionally, elastic deformation-related effects can be observed extending into the LCE bulk related to the integrated layer formation. The surface of the LCE can also be observed to have a buckled appearance (Fig. 2b) due to deswelling. Additionally, taking the layer resistivity at the saturated concentration, the average layer thickness was calculated from the changing resistance values. Both approaches yield comparable results.

For a more detailed approach, the LCE sample was reprocessed at a constant carbon particle concentration and variable surface expansion ratios A_S. The change in calculated layer thickness is shown in Fig. 1b. Without using surface expansion, a thin film of about 0.15 μm in thickness forms on the LCE surface. This value is comparable to LCE surface roughness values calculated from atomic force microscopy images of roughly 0.05 μm. It can be observed that as the surface expansion ratio increases, the layer thickness also increases rapidly. The trend line ($d \propto A_S^x$) in Fig. 1b yields an exponent $x \approx 2.7$ close to an anticipated value of $x \approx 3$ predicted by percolation theory.[39]

4. Integrated layer composition

To examine the LCE surface composition as a property of depth, X-ray photoelectron spectroscopy (XPS) was used in combination with Ar-ion sputtering. By performing Ar-ion sputtering to remove material, followed by subsequent XPS spectra acquisition, the elemental composition (C, O and Si) with depth can be investigated. The C and Si signals arise from the mesogen and elastomer polymer network, respectively. The results for C and Si are shown in Fig. 3 for the carbon particle reprocessed LCE. The C decay and Si increase give characteristic depths, d_0. The average resistivity vs. depth (inset to Fig. 3) can be estimated using Eq. 2 and the experimental d_0 value for carbon, $d_0^C \approx 300$ nm. The obtained profile is in agreement with that of SEM micrographs and resistance measurements shown previously for the carbon particle reprocessed LCE sample at around 2 μm.

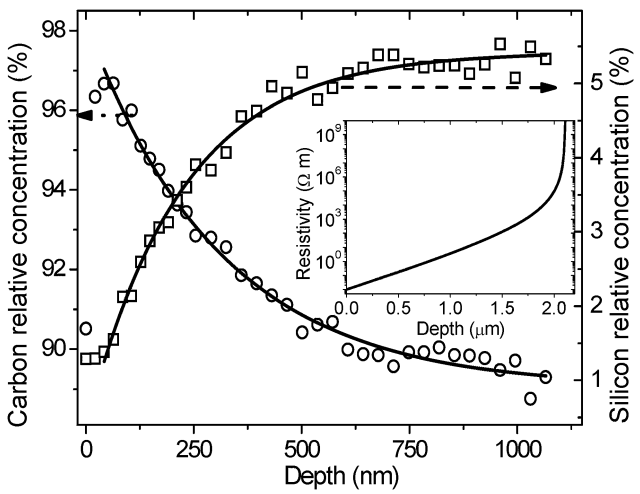

Fig. 3 Relative change in concentration of carbon (squares) and silicon (circles) as a function of the depth into the carbon black reprocessed LCE surface. The lines are single exponent fits to the respective data points. The change in resistivity per unit volume vs. depth (from the LCE surface) is shown in the inset.

5. Piezoresistance

The relative length L/L_0 measurement consisted of hanging the LCE vertically with a small static stress value inside custom made air-heating equipment, then measuring the length and resistance simultaneously as a function of temperature T, starting at high temperature. When reaching room temperature, the LCE was mechanically stretched at constant temperature, i.e. temperature induced length changes were replaced by strain-induced deformation.

For a purely geometrical change in sample shape, when an imposed deformation in the alignment direction of magnitude λ is performed, the remaining directions perpendicular to the alignment direction contract by $\lambda^{1/2}$ (Poisson ratio $\approx$ 0.5). If the integrated layer is assumed to deform as a continuum and the same as the bulk LCE, the expected relative resistance change R/R_0 of the reprocessed layer is then $R/R_0 = \lambda^2$. The observed change in R/R_0 is far greater in magnitude than λ^2 The change in particle resistivity vs. T of individual carbon particles[38] also does not support such large changes in R/R_0 vs. T. One explanation is that the composite layer resistivity ρ is allowed to change, i.e. the local volume fraction p of conducting particles changes. Here, the "local volume fraction" stands for the effective volume fraction of nanoparticles in the conducting surface layer. The relative change in the conducting layer resistivity can be described by lattice percolation theory[39] as Eq. 2. Let us assume that the deformation λ controls the percolation-related phenomena *via* $p = p_0\lambda^{-\Xi}$ where p_0 is the volume fraction at $\lambda = 1$ and Ξ is a non-linear scaling factor ($0 \leq \Xi \leq 3$). The Ξ parameter controls any non-conserving volume change experienced, as well as eventual nanoparticle–polymer interplay. Taking into account both dimensionality change and particle distributional change, the relative resistivity is then given by Eq. 3. Let us note that the above modelling assumes that the carbon particle–LCE layer behaves as a continuum upon deformation:

$$R/R_0 = \lambda^2[(p_0 - p_c)(p_0\lambda^{-\Xi} - p_c)]^{\kappa} \quad (3)$$

This demonstrates that it is the percolation phenomena and not the geometrical changes that play a dominant role in the R/R_0 vs. T behaviour. A combined plot of R/R_0 vs. λ for both the thermal stretching regime and mechanical stretching regime is shown in Fig. 4, together with the best fits to Eq. 3. These were obtained by allowing the variable Ξ to have two different values corresponding to either regime.

In the thermal extension region, for all carbon black reprocessed LCE samples, a fitting value of $\Xi = 1$ is found. In the mechanical extension region, the reprocessed LCE samples have the value of $\Xi = 0.3$. A possible explanation for the changes in the fitting parameter Ξ is in the behaviour of reprocessed LCEs. In the mechanical stretching regime it demonstrates an interplay between nanoparticles and the polymer chain, attributed to strong entangling of the carbon particle surface into the polymer network due to its irregular shape. Evidently, this interplay is also strongly affected by the symmetry of the local stress tensor: in the mechanical stretching regime where the stress is uniaxial, the value of Ξ differs substantially from its respective value in the thermal stretching regime where the locked-in internal stress is uniaxial only on the average across the sample.

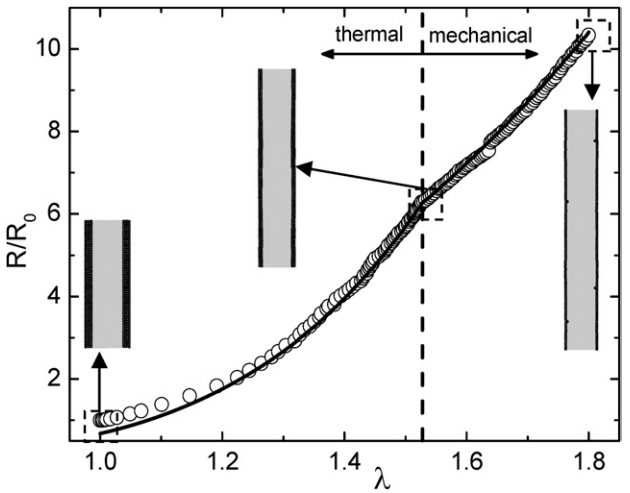

Fig. 4 Change in relative resistance R/R_0 with deformation λ for the carbon black reprocessed LCE sample. Dashed lines mark the length at which thermo-mechanical deformation was replaced with mechanical stretching (always at room temperature). The solid line is a fit with Eq. 3 (see text). Also shown is a graphical representation of the length in the average alignment direction and perpendicular thickness of the LCE. The change in concentration is described by the relative change in the density of carbon particles.

6. Actuation properties

Measurement of the L/L_0 vs. T for both reprocessed and non-reprocessed LCE samples show no observable change in the thermo-mechanical response (Fig. 5a) for any concentration or surface expansion ratio used here. The pictures of normally highly transparent unreprocessed LCE can be contrasted against the opaque reprocessed LCE at high and low T shown in Fig. 5a insert.

In order to actuate the sample *via* resistive "Joule" heating, electric current/voltage was supplied to the sample in a constant current regime. On applying DC electric power, L/L_0 vs. power dependence (Fig. 5a) was observed to be very similar to the previously recorded L/L_0 vs. T dependence. The power required for the LCE to be heated above T_{NI} and held, for the given experimental geometry, is around 80 mW.

To examine the response of reprocessed LCE, a square wave current–voltage function was applied with a time period exceeding the thermo-mechanical response time. The resulting times needed for the length of the sample to stabilise (actuation time) and return to its initial value (relaxation time) were measured (Fig. 5b). The actuation time decreases with increasing power. The relaxation time, on the other hand, remains nearly constant until approaching T_{NI} where it decreases. Above T_{NI} a linear increase with temperature is observed. This is due to the interplay between the transient heating across the LCE and the non-linear temperature response of the LCE. The applied DC signal allows the power to generate heat uniformly in the carbon layer, whereas the large surface area to volume ratio allows the heat to be efficiently and quickly transferred to the bulk of the LCE. It should be stressed that high electric and thermal conduction values of reprocessed samples are prerequisite for rapid actuation and relaxation. Increasing the power supplied and reducing the time allows for relatively fast actuation times to be used (Fig. 5b inset). A movie file showing a typical actuation response is available online.[40]

7. Degradation results

All samples were hung vertically with a fixed stress in place at room temperature. Repetitious current limited square wave

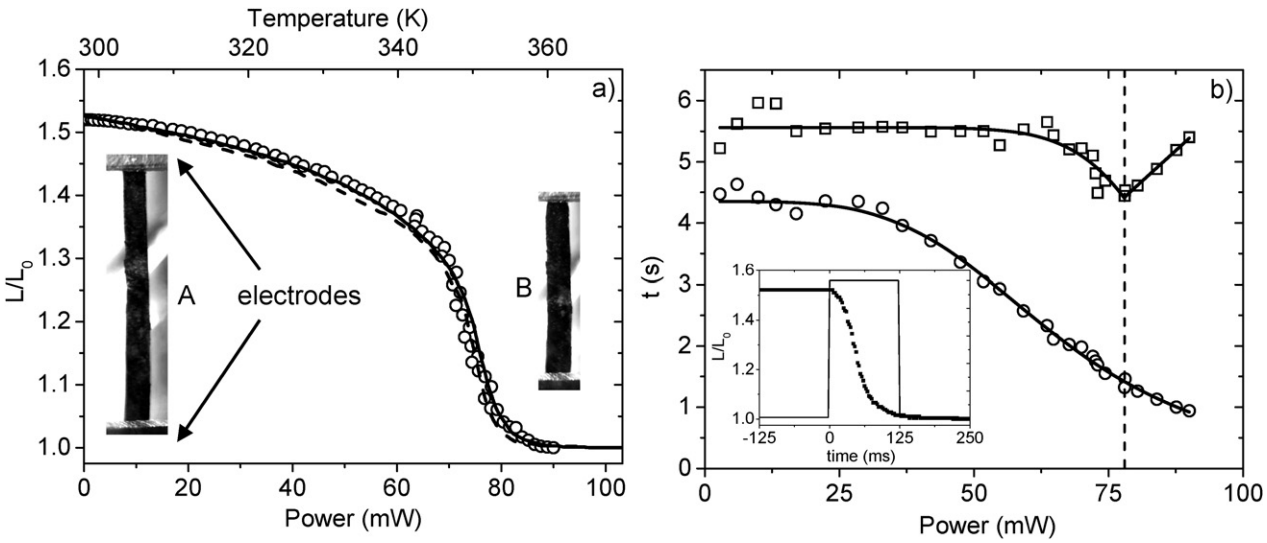

Fig. 5 a) Comparative plots of L/L_0 vs. temperature for unprocessed (dashed line) and high concentration CB reprocessed LCE (solid line) and L/L_0 vs. power (circles) for the same reprocessed LCE. Also inset are two pictures of the sample, taken at $T = 298$ K (A) and $T = 365$ K (B), showing the electrodes attached by conducting silver paste. The top electrode was fixed, whereas the bottom electrode of an appropriate mass was restricted to movement in one dimension and connected to the power source with a thin gauge conducting wire. b) Actuation times (squares) and relaxation times (circles) of the CB reprocessed sample as a response to a long time period square wave. Inset: schematic plot of the pulsed actuation (power pulse: solid line, LCE response: points) of a 125 ms high power pulse.

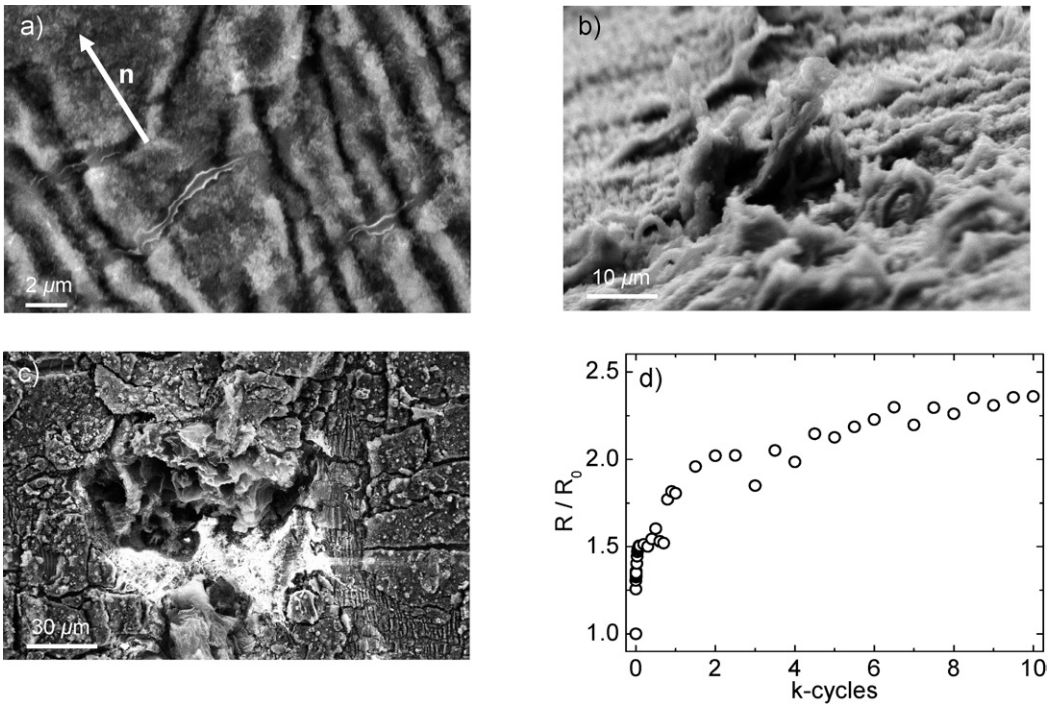

Fig. 6 SEM images of the degraded LCE samples. Images of the carbon black reprocessed LCE surface show (a) cracks in the conducting surface layer extending perpendicularly to the average alignment direction (denoted by the white arrow), (b) detachment of conducting surface material, (c) evidence of an electrical discharge (short circuit), with a cavernous indentation into the LCE interior with a diameter of around 100 μm. (d) The relative change in resistance R/R_0 as a function of the actuation cycles performed for carbon black reprocessed LCE.

pulses were applied with a repetition rate of 60 seconds (20% duty cycle). As the ageing cycles are performed, the macroscopic LCE resistance increases. The measurements were performed in a constant power mode (constant peak power at the end of the heating part of the each cycle), requiring compensation in the current.

To interpret the degradation mechanism in further detail, the degraded LCEs were examined using SEM. The reprocessed LCE surface can be observed to have cracks (Fig. 6a), where insulating LCE is visible through the highly conducting surface layer. In some areas where the surface layer is observed at an angle (Fig. 6b), some material is partially detached from the surface. The relatively good SEM image contrast proves that the LCE material is coated with carbon nanoparticles, since the LCE is intrinsically insulating. Non-actuated reprocessed LCEs as well as virgin LCEs showed no evidence of detachment at the surfaces. For reprocessed LCEs that are allowed to fail electrically, some evidence of the failure mechanism is present in the form of cavernous indentations into the internal LCE area (Fig. 6c), caused by electrical discharges. In this case the internal area is conducting to a sufficient degree to allow an SEM image to be taken. In other cases where this structure was observed, there was insufficient conductivity.

The degradation of the integrated layer resistance is observed to be a dual-timescale process (Fig. 6d). The initial few cycles are attributed to sample realignment due to swelling hysteresis, reprocessing, and the presence of a fixed stress value. Let us stress that for all samples the unadulterated bulk LCE showed no signs of degradation after 10000 heating–cooling cycles as the LCE still performed thermally induced shape changes. The degradation is therefore strictly related to the behaviour of the conducting layer.

8. Conclusions

In summary, the field of LCE is still maturing in many ways. The interplay of rubber elasticity and mesogenic ordering allows many possibilities in system design through change of the constituent components (mesogen (nematic, smectic, ferroelectric), crosslinker (rigidity, phase behaviour, functionality…), their relative ratios (crosslinking density) or the even method of the network formation (imposed stress, shearing,…). The understanding of interaction of LCE with nanoparticles is still in its infancy. An effective use of the unusual properties displayed by orientational or positional ordering and elasticity has yet to be fully utilised and the field has an exciting future.

Here, a brief overview of the field has been summarised and one method to create an effectively conducting liquid crystalline elastomer has been shown, using an existing LCE network. The resulting electro-thermo-mechanical properties have been analysed (actuation and degradation) as well as the resistive properties of CB-reprocessed LCEs subjected to strain.

Acknowledgements

The authors wish to express their gratitude to Elke Stibal-Fisher for LCE synthesis and the Ljubljana Chemistry Institute for SEM (Zeiss FE-SEM Supra 35 VP). This work was supported by EU (HPRN-CT-2002-00169) and by the Slovenian Research Agency (P1-0099 and J1-6539).

References

1 (*a*) M. Warner and E. M. Terentjev, *Liquid Crystal Elastomers* (Oxford university press) 2003; (*b*) E. M. Terentjev, Liquid-crystalline Elastomers, *J. Phys: Condens. Matter*, 1999, **11**, R239; (*c*) S. Mayer and R. Zentel, *Curr. Opin. Solid State Mater. Sci.*, 2002, **6**, 545.

2 (*a*) H. Finkelmann and H. Wermter, *ACS Abstracts*, 2000, **219**, 189; (*b*) S. V. Ahir, A. R. Tajbakhsh and E. M. Terentjev, *Adv. Funct. Mater*, 2006, **16**(4), 556.

3 J. D. W. Madden, N. A. Vandesteeg, P. A. Anquetil, P. G. A. Madden, A. Takshi, R. Z. Pytel, S. R Lafontaine, P. A. Wieringa and I. W. Hunter, *IEEE J. Oceanic Eng.*, 2004, **29**(3), 706.

4 (*a*) H. Finkelmann, E. Nishikawa, G. G. Pereira and M. Warner, *Phys. Rev. Lett.*, 2001, **87**, 015501; (*b*) P. M. Hogan, A. R. Tajbakhsh and E. M. Terentjev, *Phys. Rev. E*, 2002, **65**, 041720.

5 M. Camacho-Lopez, H. Finkelmann, P. Palffy-Muhoray and M. Shelley, *Nat. Mat.*, 2004, **3**, 307.

6 Y. Yu, M. Nakano and T. Ikeda, *Nature (London)*, 2003, **425**, 145.

7 S. S. Roy, W. Lehmann, E. Gebhard, C. Tolksdorf, R. Zentel and F. Kremel, *Mol. Cryst. Liq. Cryst.*, 2002, **375**, 253.

8 Y. Yusuf, J. H. Huh, P. E. Cladis, H. R. Brand, H. Finkelmann and S. Kai, *Phys. Rev. E*, 2005, **71**, 061702.

9 S. Courty, J. Mine, A. R. Tajbakhsh and E. M. Terentjev, *EuroPhysics Lett.*, 2003, **64**(5), 654.

10 C. M. Spillmann, B. R. Ratna and J. Naciri, *Appl. Phys. Lett.*, 2007, **90**, 021911.

11 (*a*) M. Shahinpoor, *Proc. of Society for Photo-Optical Instrumentation Engineers*, 2000, **3987**, 187; (*b*) H. Finkelmann and M. Shahinpoor, *Proc. SPIE: Electroactive Polymers and Devices*, 2002, **4695**, 147.

12 D. K. Shenoy et al., *Sen. Act. A*, 2002, **96**, 184.

13 (*a*) S. V. Ahir and E. M. Terentjev, *Nature materials*, 2005, **6**, 491; (*b*) Y. Y. Huang, S. V. Ahir and E. M. Terentjev, *Phys. Rev. B*, 2006, **73**, 125422; (*c*) S. V. Ahir, S. X. Lu, B. Panchapakesan and E. M. Terentjev, *Phys. Rev. B.*, 2007, **76**, 165437.

14 M. Winkler, A. Kaiser, S. Krause, H. Finkelmann and A. Schmidt, *Magnetoactive Liquid Crystal Elastomers*, APS march meeting proceedings, New Orleans, USA (2008).

15 (*a*) M. Warner and L. Mahadevan, *Phys.l Rev. Lett.*, 2004, **92**, 134302; (*b*) D. Corbett and M. Warner, *Phys. Rev. Lett.*, 2006, **96**, 237802; (*c*) D. Corbett and M. Warner, *Phys. Rev. Lett.*, 2007, **99**, 174302.

16 G. Skacej and C. Zannoni, to be published in *Eur. Phys. J. E* (2008).

17 J. M. Adams and M. Warner, *Phys. Rev. E*, 2008, **77**, 021702.

18 B. Mbanga and R. Selinger, *Electronic liquid crystals communications*, submitted.

19 H. Huang and F. Spaepen, *Acta mater.*, 2000, **48**, 3261.

20 (*a*) K. J. Kim and M. Shahinpoor, *Polymer*, 2002, **43**, 797; (*b*) M. Shahinpoor, Y. Bar-Cohen, J. Simpson and J. Smith, *Smart Mater. Structures Int. J.*, 1998, **7**, R15.

21 M. Chambers, B. Zalar, M. Remškar, H. Finkelmann and S. Žumer, *Appl. Phys. Lett.*, 2006, **89**, 243116.

22 M. Chambers, B. Zalar, M. Remškar, J. Kovač, H. Finkelmann and S. Žumer, *Nanotechnology*, 2007, **18**, 415706.

23 M. Chambers, B. Zalar, M. Remškar, H. Finkelmann and S. Žumer, *Nanotechnology*, 2008, **19**, 155501.

24 S. P. Lacour, S. Wagner, Z. Huang and Z. Suo, *Appl. Phys. Lett.*, 2003, **82**, 2404.

25 (*a*) G. Ausanio et al., *Sens. and Act. A*, 2006, **127**, 56; (*b*) J. E. Martin et al., *Phys Rev. B*, 2003, **67**, 094207.

26 F. El-Tantawy, K. Kamada and H. Ohnabe, *Mat. Lett.*, 2002, **56**, 112.

27 J. Küpfer and H. Finkelmann, *Macromol. Chem. Rapid Commun.*, 1991, **12**, 717.

28 J. B. Donnet, R. C. Bansal and M. J. Wang, 1993, *Carbon Black: Science and Technology, 2nd edition: revised and expanded* (Marcel Dekker inc, New York).

29 M. Doi, *Introduction to polymer physics*, (Clarendon Press, Oxford) p.63 (1996).

30 (*a*) A. Matsuyama, *J. Phys. Soc. Jap.*, 2004, **73**(4), 1070; (*b*) A. Matsuyama, *J. Chem. Phys.*, 2007, **127**, 084906.

31 (*a*) Y. Yusuf, Y. Sumisaki and M. S. Abthorpe, *Chem. Phys. Lett.*, 2003, **382**, 198; (*b*) Y. Yusuf, Y. Ono, Y. Sumisaki and S. Kai, *Mathematical Aspects of Complex Fluids III proceedings*, Rims Symposium, Kyoto, Japan; (*c*) Y. Yusuf et al., *Phys Rev. E*, 2004, **69**, 021710; (*d*) Y. Yusuf et al., *Chem. Phys. Lett.*, 2004, **389**, 443.

32 R. R. Dagastine, D. C. Prieve and L. R. White, *J. Coll. Inter. Sci.*, 2003, **249**, 78.

33 E. I. Franses et al., *Langmuir*, 1995, **11**, 3177.

34 A. Galliano, S. Bistac and Scholutz, *J. Colloid Interface sci.*, 2003, **265**, 372.

35 D. Myers. *Surfaces, Interfaces and colloids: Principles and applications* (VCH publications, New York) p. 133 (1991).

36 K. Laszlo, P. Podkoscilny and A. Dabrowski, *Langmuir*, 2003, **19**, 5287.

37 M. B. Heaney, *Appl. Phys. Lett.*, 1996, **69**, 2602.

38 P. Mandal, A. Neumann, A. G. M. Jansen, P. Wyder and R. Deltour, *Phys. Rev. B*, 1997, **55**, 452.

39 M. B. Heaney, *Physica A*, 1997, **241**, 296.

40 See EPAPS Document No. E-APPLAB-89-212650 for a movie of a reprocessed LCE undergoing an electrically induced thermal cycle within an actuation time of around 125 ms. This document can be reached *via* the EPAPS homepage (http://www.aip.org/pubservs/epaps.html).